Octupole and quadrupole modes in radon isotopes using the proton-neutron interacting boson model

O. Vallejos and J. Barea
Departamento de Física, Universidad de Concepción, Barrio Universitario, Concepción, Chile

(Received 23 November 2020; revised 3 May 2021; accepted 1 June 2021; published 8 July 2021)

We have performed a systematic study of the spectroscopic properties of the isotopic chain $^{214-226}$Rn using the *spdf*-IBM-2 interacting boson model. This model includes octupole degrees of freedom, what allows the description of negative- and positive-parity states with the same Hamiltonian. We discuss how this model is able to describe the transition from vibrational to rotational spectra in these nuclei with a rather small set of parameters, which were obtained to reproduce the properties of $^{214-222}$Rn. Then the calculations regarding ^{224,226}Rn can be considered a prediction, which compares very well with recent experimental data.

DOI: 10.1103/PhysRevC.104.014308

I. INTRODUCTION

The present study is motivated by the growing interest in finding particles with nonzero permanent electric dipole moments (EDMs). The existence of such particles would imply a violation of the time-reversal (T) symmetry at a level higher than the one present in the standard model through a phase in the Cabbiobo-Kobayashi-Maskawa matrix responsible for the mixing of the quark flavors. Thus the existence of fundamental interactions would be confirmed where the combined charge (C) and parity (P) operation would be violated, assuming that the CPT operation is a universal symmetry. Many extensions of the standard model include sources of CP violation in a natural way, such as supersymmetry theories, left- and right-handed current models, or those with multiple Higgs bosons, which in many cases are necessary to account for the imbalance between matter and antimatter observed until now.

Atoms whose nuclei with odd mass number exhibit static octupole deformation are good candidates for atomic EDM experiments, where T violation can be constrained, because the sensitivity can be enhanced 2–3 orders of magnitude through the nuclear Schiff moment [1]. In this context, radon, radium, or francium atoms have been proposed as suitable for EDM measurements [2] because their nuclei exhibit experimental signatures of octupole correlations such as alternating-parity rotational bands and enhanced $E1$ and $E3$ transitions [3–5]. Although the octupole correlations reported about them are dynamic, there are studies which show that the Schiff moments are also enhanced [6–8].

In this work we decided as a first step to study the chain $^{214-226}$Rn in a systematic way. There is only one recent study of two of these nuclei (^{214,216}Rn) using the shell model [9]. Other studies consider radon isotopes with neutron number below shell closure $N = 126$ using the shell model [10] or the nucleon pair approximation model [11]. The ^{218,220,222}Rn were also studied using the *spdf*-IBM-1 model in Refs. [12,13]. Previous studies using this model were reported in Refs. [14–17], but as far as we know none of them uses the proton-neutron degree of freedom. In our study we use the *spdf*-IBM-2 model for the first time, in which proton and neutron bosons are distinguished. There exist very few works with the octupole degree of freedom considered in which proton and neutron bosons are distinguished. In Ref. [18], *sdf*-IBM-2 is considered with emphasis on the dynamical symmetry aspects of the model, while $E1$ transitions between the 3^-_1 and $2^+_{1,\mathrm{ms}}$ states are studied in Ref. [19]. In addition there is a work [20] using *sdfg*-IBM-2 where one f boson is considered in the calculations. More recently *sdf*-IBM-1 based in energy density theory has been applied to study phase transitions in light actinide and rare-earth nuclei [21] and *spdf*-IBM-1 has been used to unveil possible double octupole phonon structure in ^{240}Pu [22]. In our work we aim to obtain a nuclear structure picture of the isotopes under study from a phenomenological point of view. In addition, our study represents a systematic study of even-even radon isotopes from ^{214}Rn to ^{226}Rn for the first time, apparently beyond the capabilities that the shell model can reach today without a sizable truncation of the space model for the heaviest isotopes in the chain. The calculations were performed considering the experimental information up to ^{222}Rn. Just very recently experimental information on ^{224}Rn and ^{226}Rn has been released [23] and our results compare extremely well with the experimental data.

II. THE *spdf*-IBM2 MODEL

The interacting boson model is a model designed to describe collective properties in atomic nuclei. This can be considered an approximation of the shell model and there exist several different ways to connect both models when proton and neutron bosons are distinguished, as we do in this work. Usually correlated pairs of valence nucleons coupled to the integer angular momenta L and the parity π are treated as bosons that can occupy orbitals characterized by the same values of angular momenta and parity. Then the ground state and the low-lying states in even-even nuclei are obtained from interactions between a system of N bosons allowed to occupy the abovementioned orbitals, where N is the total number of valence nucleons divided by 2.

In the *spdf*-IBM-2 model the bosons are allowed to occupy the four orbitals $L^\pi = 0^+, 1^-, 2^+$, and 3^-, which motivates us to call those in each orbital s, p, d, and f bosons. As we mentioned proton and neutron bosons are distinguished, which corresponds to correlated pairs of protons and neutrons, respectively. Using a second quantization formulation, creation and annihilation operators are introduced for each orbital as $s^\dagger_\rho$, $p^\dagger_{\rho,\alpha}$, $d^\dagger_{\rho,\beta}$, and $f^\dagger_{\rho,\gamma}$ and as s_ρ, $p_{\rho,\alpha}$, $d_{\rho,\beta}$, and $f_{\rho,\gamma}$, where $\rho = \pi$ is for protons and $\rho = \nu$ is for neutrons, and

$$\alpha = -1, 0, 1, \tag{1}$$

$$\beta = -2, -1, 0, 1, 2, \tag{2}$$

$$\gamma = -3, -2, -1, 0, 1, 2, 3 \tag{3}$$

are the magnetic quantum numbers. These operators satisfy Bose commutation relations. The algebraic structure of the model corresponds to $U_\pi(16) \times U_\nu(16)$. To write the Hamiltonian of the system, spherical tensor operators are used for the annihilation operators:

$$\tilde{s}_\rho = s_\rho, \tag{4}$$

$$\tilde{p}_{\rho,\alpha} = (-1)^\alpha p_{\rho,-\alpha}, \tag{5}$$

$$\tilde{d}_{\rho,\beta} = (-1)^\beta d_{\rho,-\beta}, \tag{6}$$

$$\tilde{f}_{\rho,\gamma} = (-1)^\gamma f_{\rho,-\gamma}. \tag{7}$$

The most general Hamiltonian contains a huge number of terms and hence parameters. We used a restricted version based in the Talmi Hamiltonian [24], which reduces drastically the number of parameters:

$$\hat{H} = \varepsilon_p(\hat{n}_{p_\pi} + \hat{n}_{p_\nu}) + \varepsilon_d(\hat{n}_{d_\pi} + \hat{n}_{d_\nu}) + \varepsilon_f(\hat{n}_{f_\pi} + \hat{n}_{f_\nu}) + \kappa \hat{Q}^{(2)}_\pi \cdot \hat{Q}^{(2)}_\nu + \hat{M}_{\pi\nu}. \tag{8}$$

This Hamiltonian is the natural extension of the one used in Ref. [12] to include proton-neutron degrees of freedom. Here the number operators read as $\hat{n}_{p_\rho} = -p^\dagger_\rho \cdot \tilde{p}_\rho$, $\hat{n}_{d_\rho} = d^\dagger_\rho \cdot \tilde{d}_\rho$, and $\hat{n}_{f_\rho} = -f^\dagger_\rho \cdot \tilde{f}_\rho$, and ε_p, ε_d, and ε_f are the boson energies with respect to the s boson energy. We take $\varepsilon_p = \varepsilon_f$ because microscopic considerations in Refs. [16,17] suggest that the dipole and octupole pairs occur at the same order of magnitude in the intrinsic state. Actually these references justify the use of a p boson to simulate the appearance of a dipole nucleon pair with finite probability in the intrinsic state when a Hamiltonian with spherical, quadrupole, and octupole mean fields is used. $\hat{Q}^{(2)}_\rho$ is the quadrupole operator:

$$\hat{Q}^{(2)}_\rho = [s^\dagger_\rho \tilde{d}_\rho + d^\dagger_\rho \tilde{s}_\rho]^{(2)} + \chi_\rho [d^\dagger_\rho \tilde{d}_\rho]^{(2)} + \chi'_\rho [p^\dagger_\rho \tilde{f}_\rho + f^\dagger_\rho \tilde{p}_\rho]^{(2)} + \chi''_\rho [p^\dagger_\rho \tilde{p}_\rho + f^\dagger_\rho \tilde{f}_\rho]^{(2)}, \tag{9}$$

where χ_ρ, χ'_ρ, and χ''_ρ are free parameters and $\hat{M}_{\pi\nu}$ is the so-called *Majorana* operator:

$$\hat{M}_{\pi\nu} = \xi_{sp}\hat{M}_{sp} + \xi_{sd}\hat{M}_{sd} + \xi_{sf}\hat{M}_{sf} + \xi_{dp}\hat{M}_{dp} + \xi_{df}\hat{M}_{df}, \tag{10}$$

where ξ_{sp}, ξ_{sd}, ξ_{sf}, ξ_{dp}, and ξ_{df} are free parameters and

$$\hat{M}_{sp} = [s^\dagger_\pi p^\dagger_\nu - s^\dagger_\nu p^\dagger_\pi]^{(1)} \cdot [\tilde{s}_\pi \tilde{p}_\nu - \tilde{s}_\nu \tilde{p}_\pi]^{(1)} - 2[d^\dagger_\nu p^\dagger_\pi]^{(1)} \cdot [\tilde{d}_\nu \tilde{p}_\pi]^{(1)}, \tag{11}$$

$$\hat{M}_{sd} = [s^\dagger_\pi d^\dagger_\nu - s^\dagger_\nu d^\dagger_\pi]^{(2)} \cdot [\tilde{s}_\pi \tilde{d}_\nu - \tilde{s}_\nu \tilde{d}_\pi]^{(2)} - 2\sum_{k=1,3}[d^\dagger_\nu d^\dagger_\pi]^{(k)} \cdot [\tilde{d}_\nu \tilde{d}_\pi]^{(k)}, \tag{12}$$

$$\hat{M}_{sf} = [s^\dagger_\pi f^\dagger_\nu - s^\dagger_\nu f^\dagger_\pi]^{(3)} \cdot [\tilde{s}_\pi \tilde{f}_\nu - \tilde{s}_\nu \tilde{f}_\pi]^{(3)} - 2\sum_{k=1,3,5}[f^\dagger_\nu f^\dagger_\pi]^{(k)} \cdot [\tilde{f}_\nu \tilde{f}_\pi]^{(k)}, \tag{13}$$

$$\hat{M}_{dp} = \sum_{k=1}^{3}[d^\dagger_\pi p^\dagger_\nu - d^\dagger_\nu p^\dagger_\pi]^{(k)} \cdot [\tilde{d}_\pi \tilde{p}_\nu - \tilde{d}_\nu \tilde{p}_\pi]^{(k)}, \tag{14}$$

$$\hat{M}_{df} = \sum_{k=1}^{5}[d^\dagger_\pi f^\dagger_\nu - d^\dagger_\nu f^\dagger_\pi]^{(k)} \cdot [\tilde{d}_\pi \tilde{f}_\nu - \tilde{d}_\nu \tilde{f}_\pi]^{(k)}. \tag{15}$$

$\hat{M}_{sd}$ is identical to the Majorana operator in the *sd*-IBM-2. $\hat{M}_{sp}$ and $\hat{M}_{sf}$ are similar, but replacing the d-boson operator with the p-boson and f-boson operators, respectively, as it was done in Ref. [25] for the g-boson operator. $\hat{M}_{df}$ was used in Ref. [18] and $\hat{M}_{dp}$ is similar, but replacing the f-boson operator with the p-boson operator. The full Majorana operator should include additional terms, but we postulate $\xi_{sp} = \xi_{sf}$ and $\xi_{dp} = \xi_{df}$ to reduce the number of free parameters and to consider finally only three independent parameters.

TABLE I. Values in MeV of the parameters used in this work.

Nucleus	ε_d	$\varepsilon_{p,f}$	κ
^{214}Rn	0.61	0.95	−0.001
^{216}Rn	0.40	0.94	−0.001
^{218}Rn	0.38	0.94	−0.030
^{220}Rn	0.37	0.92	−0.050
^{222}Rn	0.36	0.90	−0.050
^{224}Rn	0.35	0.88	−0.050
^{226}Rn	0.34	0.86	−0.050

III. RESULTS AND DISCUSSION

We have applied the *spdf*-IBM-2 model to the isotopic chain $^{214-226}$Rn without any restriction in the number of bosons of each kind, in contrast with other studies where, for example, the number of p and f bosons is limited to one [13]. In Table I we quote in MeV the values of ε_d, $\varepsilon_p = \varepsilon_f$ and κ which change from one nucleus to another. Their evolution is smooth except for the jump given by ε_d from ^{214}Rn to ^{216}Rn. The values of ε_d and $\varepsilon_p = \varepsilon_f$ for ^{224,226}Rn were obtained following the linear behavior of the values for $^{218-222}$Rn while the value of κ was maintained constant to −0.050 MeV, also following the same trend in $^{220-222}$Rn. Note that $\varepsilon_p = \varepsilon_f > \varepsilon_d$ guarantees that yrast states with $J^\pi = 1^-$ and $J^\pi = 3^-$ have similar energies that are above the energy of the first excited state $J^\pi = 2^+$. The values of the rest of the parameters remain fixed and their values are $\chi_\pi = \chi_\nu = -1.3$, $\chi'_\pi = \chi'_\nu = -1.3$,

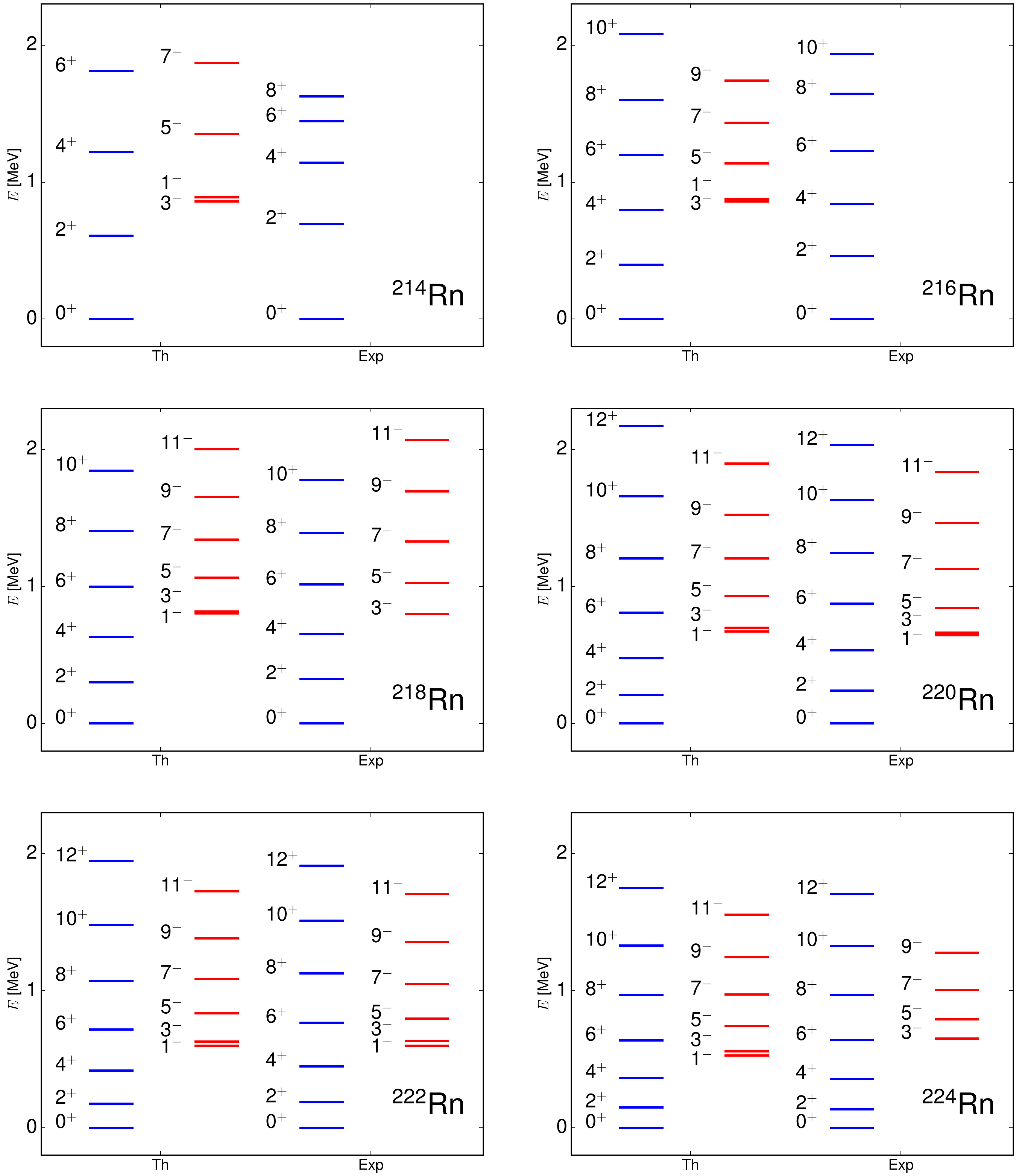

FIG. 1. Each subfigure shows calculated (left) and experimental (right) level energies of yrast states below 2 MeV. The experimental data were taken from Refs. [23,26–30].

$\chi''_\pi = \chi''_\nu = -1.3$, $\xi_{sd} = 0.07$ MeV, $\xi_{sp} = \xi_{sf} = 0.02$ MeV, and $\xi_{dp} = \xi_{df} = 0.10$ MeV.

In Figs. 1 and 2 we show the calculated and experimental level energies. The experimental level schemes for both parities are well reproduced in general. The mean deviation between calculated and experimental energies is below 0.5 MeV. Only large differences are observed in ^{214}Rn, whose level scheme deviates from a vibrational spectrum as angu-

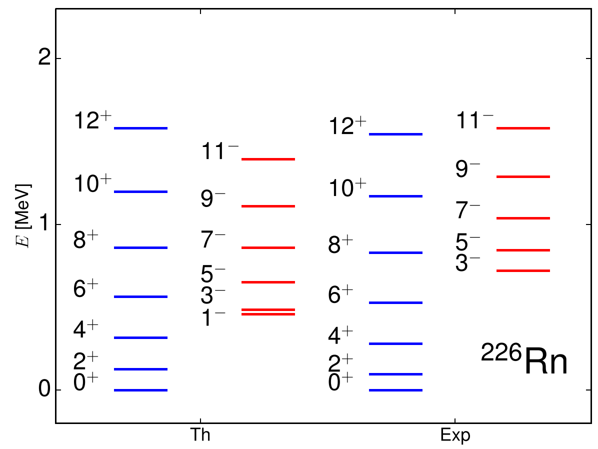

FIG. 2. Same as Fig. 1, but here for ^{226}Rn. The experimental data were taken from Ref. [23].

lar momentum increases, in contrast to, for example, ^{216}Rn, whose level scheme is pretty similar to the one found in a vibrator. The peculiar spectrum of ^{214}Rn also happens in the isotone chain $N = 128$ to which it belongs, something which deserves a separate study with a different Hamiltonian or using an extended set of parameters. In this work we followed the premise to keep the parametrization as simple as possible. For the rest of the nuclei the energy levels are well reproduced, as was mentioned earlier, where a transition from vibrational to rotational patterns is observed. With respect to the negative-parity states, experimental information in ^{214}Rn and ^{216}Rn is absent. However there are reported states without angular momentum and parity assignments that eventually could correspond to our calculations. ^{218}Rn is the first nuclide which shows a negative-parity band starting at 3^-, although our calculations show the same band starting at 1^-. This could be solved taking different values for ε_p and ε_f with $\varepsilon_p > \varepsilon_f$ for this particular nucleus, but we prefer to follow the systematic behavior of the parameters. In ^{220}Rn and ^{222}Rn the negative-parity band starts at 1^-, almost degenerate with the 3^- member of this band, which is nicely reproduced by our calculations, except in ^{224}Rn and ^{226}Rn. The energy levels of these nuclei were not used in the fitting process, because at the time of performing the calculations experimental information was absent. However we are aware of a recent publication [23] where experimental information about these nuclei is published. We calculated their level energies by extrapolating the values of the parameters obtained in lighter nuclides, as we mentioned at the beginning of this section. We can observe that this extrapolation works fine in ^{224}Rn for both parities, but negative-parity states in ^{226}Rn are underestimated with respect to the experimental values.

TABLE III. Values of the parameters used in $Q^{(1)}$ and $Q^{(3)}$.

L	$\alpha_\pi^{(L)}$	$\beta_\pi^{(L)}$	$\gamma_\pi^{(L)}$	$\alpha_\nu^{(L)}$	$\beta_\nu^{(L)}$	$\gamma_\nu^{(L)}$
1	−1.5	−1.9	1.2	−1.3	−1.6	1.5
3	−50	58	−72	−91	68	−191

Aside from the energy levels, we have calculated some electric transition probabilities. In Table II we show the reduced transition probabilities $B(E1)$ in Weisskopf units (W.u.) calculated using the following operator:

$$Q^{(1)} = e_\pi^{(1)} Q_\pi^{(1)} + e_\nu^{(1)} Q_\nu^{(1)}, \tag{16}$$

where $e_\pi^{(1)} = e_\nu^{(1)} = 1\,e$ fm are bosonic charges, and

$$\hat{Q}_\rho^{(1)} = \alpha_\rho^{(1)}[p_\rho^\dagger \tilde{s}_\rho + s_\rho^\dagger \tilde{p}_\rho]^{(1)} + \beta_\rho^{(1)}[p_\rho^\dagger \tilde{d}_\rho + d_\rho^\dagger \tilde{p}_\rho]^{(1)} + \gamma_\rho^{(1)}[d_\rho^\dagger \tilde{f}_\rho + f_\rho^\dagger \tilde{d}_\rho]^{(1)}, \tag{17}$$

with $\alpha_\rho^{(1)}$, $\beta_\rho^{(1)}$, and $\gamma_\rho^{(1)}$ being parameters that allow us to specify the relative weight of each term in $\hat{Q}_\rho^{(1)}$. Both the bosonic charges and these parameters were kept fixed for all the nuclides in the chain. In Table III the values of the parameters are quoted. These were obtained using the Otsuka-Arima-Iachello (OAI) method [32] to map the shell model operator $\hat{Q}_{\mathrm{SM}}^{(1)}$ to $\hat{Q}^{(1)}$ following the same steps in Ref. [33]. More details can be found in the Appendix. We observe that the calculated values are less than 10^{-1} single-particle units (spu), typically around 10^{-2} spu, except the transition $3^- \to 4^+$, which is strongly hindered. When we compare the calculated values with the experimental information in ^{220}Rn the agreement is reasonable in terms of the order of magnitude. More experimental information would be desirable to confirm if our calculations are accurate.

Table IV shows the reduced transition probabilities $B(E2)$ along with experimental data and values calculated using the shell model (SM) only for ^{214}Rn and ^{216}Rn. Our calculated quantities were obtained using the quadrupole operator

$$\hat{Q}^{(2)} = e_\pi^{(2)} \hat{Q}_\pi^{(2)} + e_\nu^{(2)} \hat{Q}_\nu^{(2)}, \tag{18}$$

where $\hat{Q}_\rho^{(2)}$ $(\rho = \pi, \nu)$ is given in Eq. (9) and the values of the parameters χ_ρ, χ'_ρ, and χ''_ρ are the same as those used in the Hamiltonian of Eq. (8) to obtain the states and their energies.

TABLE II. $B(E1)$ transition probabilites in Weisskopf units between states of the negative-parity band and the ground-state band. Experimental data of ^{220}Rn were found in Ref. [31].

J_i^π	J_f^π	^{214}Rn	^{216}Rn	^{218}Rn	^{220}Rn (Expt.)	^{220}Rn	^{222}Rn	^{224}Rn	^{226}Rn
1^-	0^+	1.75×10^{-1}	8.67×10^{-2}	3.84×10^{-2}	$<1.5 \times 10^{-3}$	6.34×10^{-3}	8.09×10^{-4}	7.81×10^{-4}	7.76×10^{-3}
1^-	2^+	7.98×10^{-2}	2.87×10^{-2}	2.95×10^{-2}	$<3 \times 10^{-3}$	8.43×10^{-3}	2.57×10^{-3}	3.76×10^{-6}	2.52×10^{-3}
3^-	2^+	3.65×10^{-3}	4.19×10^{-3}	3.74×10^{-3}	$<20 \times 10^{-4}$	4.05×10^{-4}	7.17×10^{-5}	3.02×10^{-6}	1.72×10^{-6}
3^-	4^+	5.37×10^{-7}	1.62×10^{-7}	4.17×10^{-6}		3.63×10^{-5}	5.83×10^{-5}	4.20×10^{-5}	1.67×10^{-5}
5^-	4^+	7.54×10^{-3}	7.98×10^{-3}	2.40×10^{-3}	$3.0^{+2}_{-1.6} \times 10^{-5}$	6.07×10^{-5}	3.29×10^{-4}	4.37×10^{-4}	4.14×10^{-4}
7^-	6^+	1.16×10^{-2}	1.22×10^{-2}	1.68×10^{-3}	$<500 \times 10^{-3}$	2.78×10^{-3}	4.30×10^{-3}	4.03×10^{-3}	3.23×10^{-3}

TABLE IV. $B(E2)$ transition probabilites in Weisskopf units between states of the ground-state band and between states of the negative-parity band. The experimental data were taken from Refs. [26,28,30,31]. Values calculated with the shell model (SM) [9] are also quoted for comparison purposes. Values calculated with the IBM in ^{214}Rn that involve the $J^\pi = 10^+$ state are absent because 8 is the maximum value of the angular momentum for positive-parity states that *spdf*-IBM-2 can compute for this nucleus. Also, values calculated with IBM in ^{214}Rn and ^{216}Rn that involve the states $J^\pi = 8^+$ and $J^\pi = 10^+$, respectively, are absent because the corresponding model spaces are strongly reduced, which makes them not reliable.

		^{214}Rn			^{216}Rn		^{218}Rn		^{220}Rn		^{222}Rn		^{224}Rn	^{226}Rn
J_i^π	J_f^π	Expt.	IBM	SM	IBM	SM	Expt.	IBM	Expt.	IBM	Exp.	IBM	IBM	IBM
2^+	0^+	>0.03	13	17	17	29	>23	26	48 ± 3	40	58 ± 4	52	65	81
4^+	2^+	>0.28	17	23	25	41		43	63 ± 3	68		87	109	134
6^+	4^+	3.8^{17}_{-9}	13	22	26	41		48	73 ± 8	76		101	127	157
8^+	6^+	3.3^{+3}_{-1}		16	17	10		42		72		100	131	164
10^+	8^+	2.9 ± 0.7		6		3		26		57		89	124	160
3^-	1^-		3		3			7	60^{+50}_{-30}	7		7	8	7
5^-	3^-		8		12			19	60^{+100}_{-50}	25		31	38	45

We fixed the bosonic charges as $e_\pi^{(2)} = e_\nu^{(2)} = 18\, e\, \text{fm}^2$ for all the nuclides in the chain. This value is the usual one in this region of the chart of nuclides [12]. We can see that the values obtained follow an increasing trend, according to a transition from a vibrational to a deformed regime. The agreement of our calculations with the experimental data is remarkable for the positive-parity states. However the calculations provide smaller values than the experimental ones for the negative-parity states in the only case where we found experimental data, which is ^{220}Rn. Actually the calculated values for the transition $3^- \to 1^-$ are systematically smaller than the rest of the calculated quantities. This indicates that the structure of the 1^- and 3^- states are rather different, as we will see shortly in the discussion of the reduced transition probabilities $B(E3)$. When we compare our calculations with those obtained using the shell model, we observe that our data are slightly smaller and then closer to the experimental value in the transition $6^+ \to 4^+$ in ^{214}Rn, at least.

Also, we have calculated the reduced transition probabilities $B(E3)$, which are important to unveil octupole correlations, using the operator

$$\hat{Q}^{(3)} = e_\pi^{(3)} \hat{Q}_\pi^{(3)} + e_\nu^{(3)} \hat{Q}_\nu^{(3)}, \tag{19}$$

where $e_\pi^{(3)} = 2\, e\, \text{fm}^3$ and $e_\nu^{(3)} = 6\, e\, \text{fm}^3$, and

$$\hat{Q}_\rho^{(3)} = \alpha_\rho^{(3)} [f_\rho^\dagger \tilde{s}_\rho + s_\rho^\dagger \tilde{f}_\rho]^{(3)} + \beta_\rho^{(3)} [p_\rho^\dagger \tilde{d}_\rho + d_\rho^\dagger \tilde{p}_\rho]^{(3)} + \gamma_\rho^{(3)} [f_\rho^\dagger \tilde{d}_\rho + d_\rho^\dagger \tilde{f}_\rho]^{(3)}. \tag{20}$$

In Table V we show our calculated values along with experimental data only for ^{220}Rn. The values of the bosonic charges were fitted to reproduce the order of magnitude of the experimental data measured in ^{220}Rn, and they are the same for all the nuclides of the chain. The parameters $\alpha_\rho^{(3)}$, $\beta_\rho^{(3)}$, and $\gamma_\rho^{(3)}$ also are kept fixed for all the nuclides and were obtained using the same method used to obtain $\alpha_\rho^{(1)}$, $\beta_\rho^{(1)}$, and $\gamma_\rho^{(1)}$ in Eq. (16), which is explained in the Appendix. The calculated data show increasing values with A in the transition $3^- \to 2^+$, which indicates a change of the structure of the 3^- state. In fact, the d-boson content of these states increases when A increases, as will be explained later. In contrast, the transition $1^- \to 2^+$ is hindered in general and exhibits again the very different behavior of the 1^- state with respect to the 3^- state. In this case the 2^+ states are made of s and d bosons, while the contents of the 1^- states are essentially s and p bosons and d bosons to a lesser extent. Then the $E3$ strength between these states is small because contributions arise only from terms like $d_\rho^\dagger \tilde{p}_\rho$ in the $E3$ operator. The terms $d_\rho^\dagger \tilde{f}_\rho$ or $s_\rho^\dagger \tilde{f}_\rho$ provide very small values and the rest of them contribute nothing. The rest of the transitions show values with small variations around 80, 55, 40, and 25 W.u., except for ^{214}Rn, where the values are smaller. In the case of ^{220}Rn we can observe that our calculated value for the transition $3^- \to 0^+$ is higher than the experimental value, while for the transition $5^- \to 2^+$ the calculated value is found between the error bars. Eventually the comparison between calculated and experimental data may improve by choosing different values

TABLE V. $B(E3)$ transition probabilites in Weisskopf units between states of the negative-parity band and the ground-state band. Experimental data of ^{220}Rn were found in Ref. [31].

J_i^π	J_f^π	^{214}Rn	^{216}Rn	^{218}Rn	^{220}Rn (Expt.)	^{220}Rn	^{222}Rn	^{224}Rn	^{226}Rn
3^-	0^+	49	73	78	33 ± 4	77	81	85	91
5^-	2^+	31	52	60	90 ± 50	54	56	54	52
7^-	4^+	16	35	39		40	43	42	39
9^-	6^+	0	18	22		26	32	32	30
1^-	2^+	3	5	2	<760	1.5	1	1	1
3^-	2^+	83	91	120	<1400	165	178	192	207

TABLE VI. $B(M1)$ transition probabilites in Weisskopf units between some states of positive and negative parity.

J_i^π	J_f^π	^{214}Rn	^{216}Rn	^{218}Rn	^{220}Rn	^{222}Rn	^{224}Rn	^{226}Rn
0_1^+	1_1^+	6.87×10^{-6}	2.78×10^{-5}	4.76×10^{-2}	2.24×10^{-1}	2.97×10^{-1}	3.76×10^{-1}	0
2_1^+	1_1^+	3.99×10^{-6}	1.15×10^{-5}	1.47×10^{-2}	4.98×10^{-2}	5.87×10^{-2}	6.63×10^{-2}	0
2_1^+	2_2^+	2.51×10^{-1}	2.82×10^{-1}	1.15×10^{-3}	3.60×10^{-5}	1.50×10^{-5}	1.92×10^{-4}	5.50×10^{-4}
1_1^-	1_2^-	8.35×10^{-2}	7.51×10^{-2}	4.35×10^{-2}	2.04×10^{-2}	1.23×10^{-2}	5.79×10^{-3}	2.21×10^{-3}
1_1^-	2_1^-	3.15×10^{-7}	3.32×10^{-7}	2.52×10^{-3}	7.72×10^{-3}	1.19×10^{-2}	1.57×10^{-2}	1.92×10^{-2}
3_1^-	3_2^-	5.01×10^{-1}	5.64×10^{-1}	4.77×10^{-1}	1.23×10^{-4}	2.73×10^{-5}	2.27×10^{-4}	4.32×10^{-4}

for the parameters $\alpha_\rho^{(3)}$, $\beta_\rho^{(3)}$, and $\gamma_\rho^{(3)}$, but more experimental data would be necessary to follow this step.

Regarding the magnetic properties, we have calculated the reduced transition probabilities $B(M1)$ between some selected states, of both positive and negative parity. The magnetic dipole operator used is

$$T^{(M1)} = \sqrt{\frac{3}{4\pi}}(g_\pi \hat{L}_\pi + g_\nu \hat{L}_\nu), \tag{21}$$

where

$$\hat{L}_\rho = \sqrt{2}[p_\rho^\dagger \tilde{p}_\rho]^{(1)} + \sqrt{10}[d_\rho^\dagger \tilde{d}_\rho]^{(1)} + 2\sqrt{7}[f_\rho^\dagger \tilde{f}_\rho]^{(1)} \tag{22}$$

is the angular momentum operator [15] and the effective proton and neutron boson g factors $g_\pi = 0.63$ and $g_\nu = 0.05$ were taken from Ref. [34]. Table VI shows the results of our calculations. We can see that the transitions between the ground and the first excited state to the 1_1^+ state are hindered in

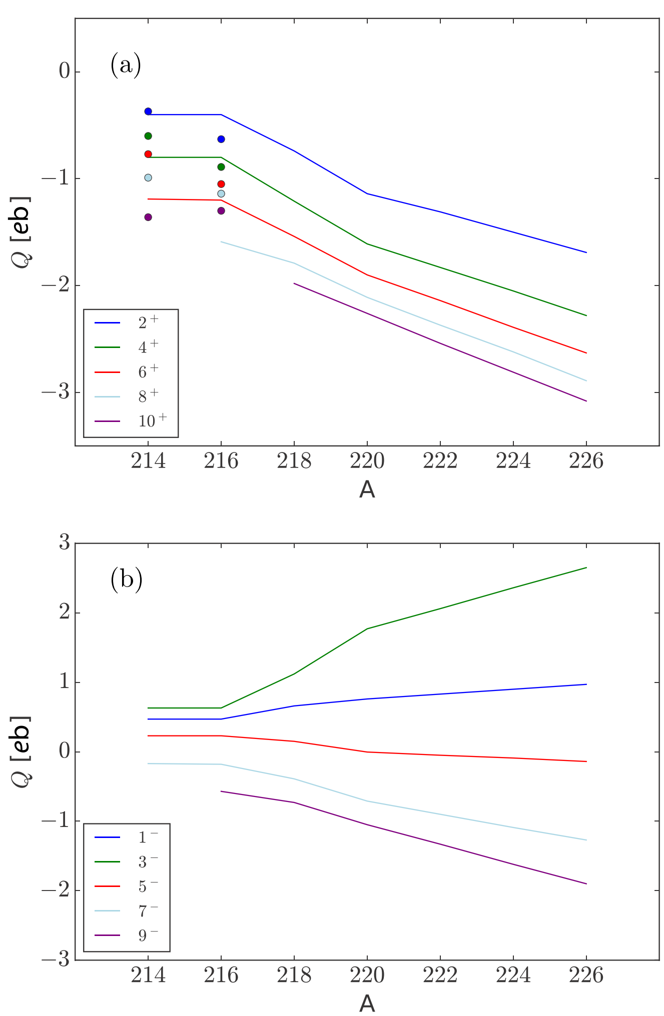

FIG. 3. Quadrupole moments in electron barns of positive (a) and negative (b) states. Lines correspond to our work and dots to shell model values [9].

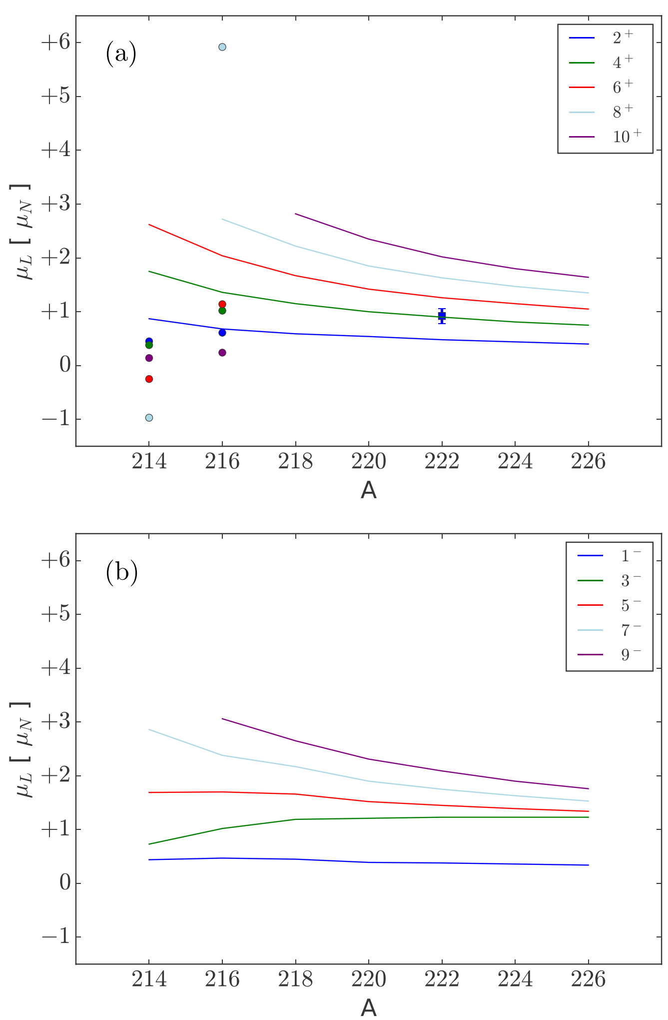

FIG. 4. Magnetic dipole moments in μ_N of positive (a) and negative (b) states. Lines correspond to our work and dots to shell model values [9]. The experimental point corresponding to ^{222}Rn was taken from Ref. [30].

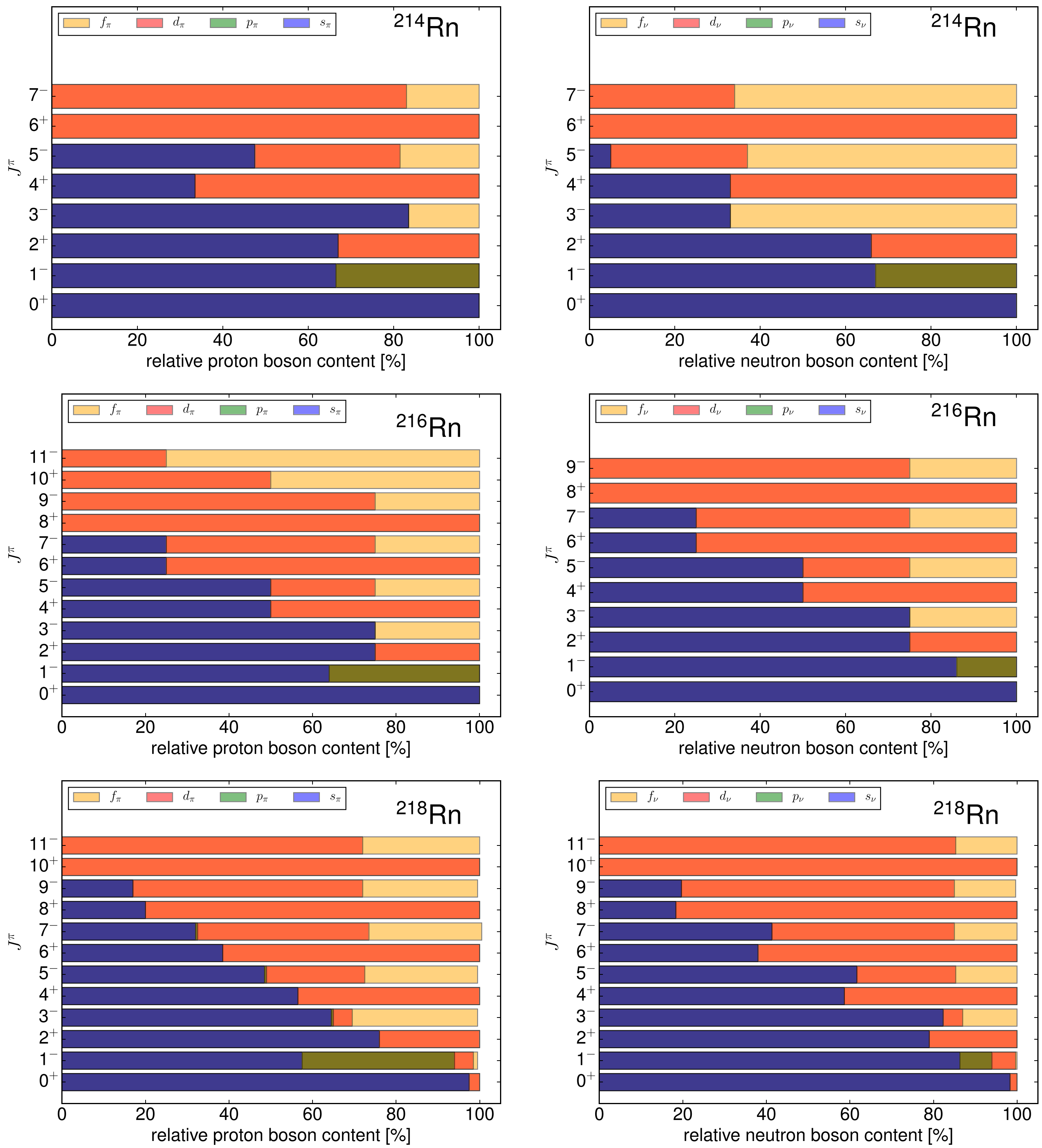

FIG. 5. s- (blue), p- (green), d- (red), and f-boson (orange) contents for protons and neutrons of the low-lying states, for positive as well as negative parity in ^{214,216,218}Rn.

the lightest isotopes, while they are of the order of the tenths for the ground states and 1 order of magnitude less for the 2_1^+ states in ^{218}Rn and heavier isotopes. In ^{226}Rn these transitions are forbidden, which indicates that the 1_1^+ state changed its structure in this nucleus. The transitions between the 2^+ states, however, show the opposite behavior, where the values decrease as we move to the heavier isotopes. This trend also happens between the 3^- states, but the transitions between the

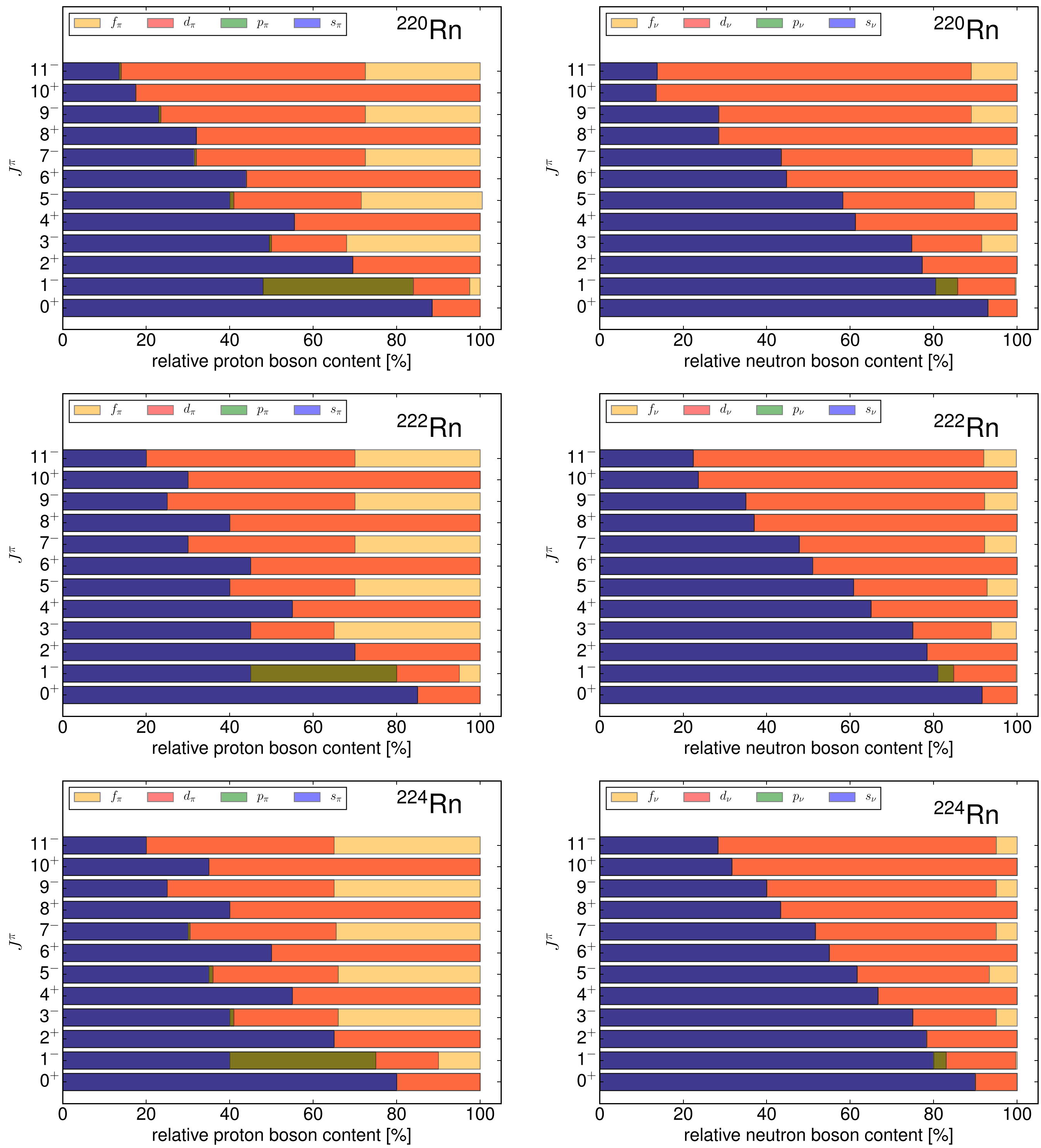

FIG. 6. Same as Fig. 5, but here for ^{220,222,224}Rn.

1^- and the 2^- states show again an increasing trend in the values, as happens for the transitions where the 1^+ state is involved. Only the transitions between the 1^- states maintain a smooth and slowly decreasing behavior as we move to the heavier isotopes.

In addition to the electromagnetic transition probabilities we have calculated the electric quadrupole moments and the magnetic dipole moments for both positive- and negative-parity states. They are shown in Figs. 3 and 4, respectively. The general trend in the quadrupole moment is the increase

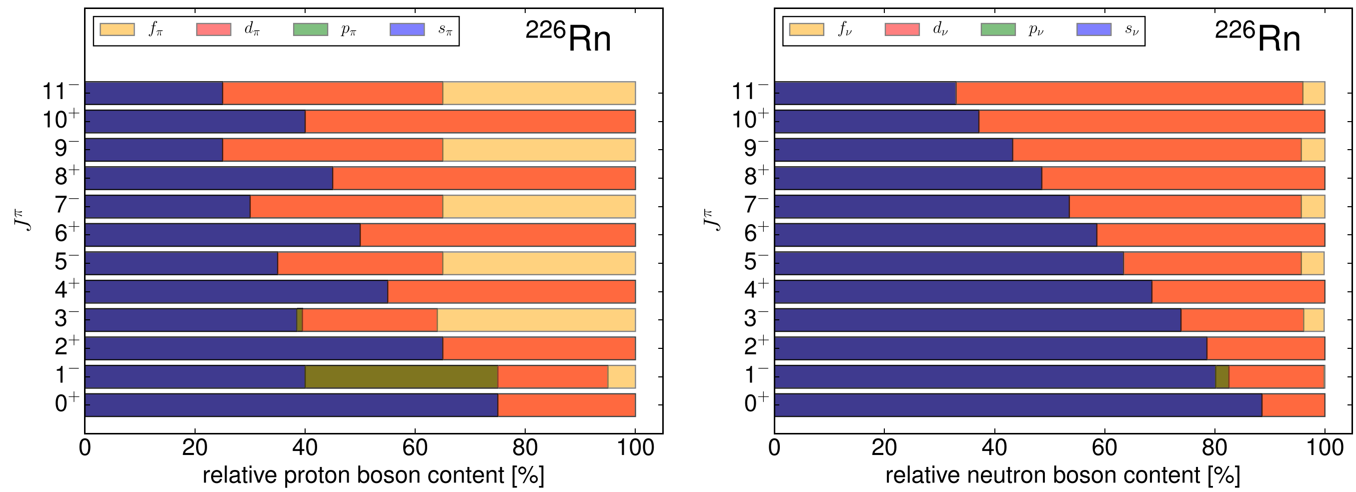

FIG. 7. Same as Fig. 5, but here for ^{226}Rn.

in the absolute values with mass number A, according to the increase in deformation as the nuclei move away the shell closure at $N = 128$. This behavior also happens for the values calculated with the shell model for all the positive-parity states except $J^\pi = 10^+$. Also, they compare well with our calculated values. All the values are negative for positive-parity states, while they are positive for the 1^- and 3^- states, negative for the 7^- and 9^- states, and positive close to zero for the 5^- states in ^{214}Rn, ^{216}Rn, and ^{218}Rn and negative in ^{220}Rn, ^{222}Rn, and ^{224}Rn. Also, the absolute values for the positive-parity states increase with the angular momenta systematically. This effect is absent in the negative-parity states, where the maximum values are dominated by the 3^- states for all the nuclei. We omitted the values of the quadrupole and magnetic moments in ^{214}Rn and ^{216}Rn for the states with the highest value of J, because the subspace associated with them is strongly reduced and the calculations where they are involved are not reliable. Regarding the magnetic moment, their values show a smooth and decreasing behavior for the positive-parity states, while the values corresponding to the negative-parity states show a different trend, where they seem to converge to a value below $2\mu_N$ in ^{224}Rn for all the angular momenta except 1^-, which shows a rather constant value around $0.4\mu_N$. When we compare our results with those from the shell model for the positive-parity states in ^{214}Rn and ^{216}Rn, we find some discrepancies. Our values are higher in general. Also, there is an experimental value in ^{222}Rn which is slightly higher than the value we calculated.

Finally we show the s-, p-, d-, and f-boson contents of the low-lying states, both for positive and negative parity, in Figs. 5–7. In the proton case, there is a clear pattern for the negative-parity states with $J \geqslant 3$ where the sum of the s_π- and d_π-boson contents is almost the same around 70% and the rest correspond to f_π-boson content. This ratio changes slightly in ^{214}Rn, where the f_π-boson content reduces to less than 20%. The relative proton boson content in the 1^- states is different and changes with A. In the lightest isotopes, ^{214}Rn and ^{216}Rn, there is 65% s_π-boson content and the rest correspond to p_π-boson content. When A increases d_π- and f_π-boson contents appear, which increase with A. This very different structure between the 1^- and the 3^- states, which also happens in the neutron sector, explains the different behavior of the electromagnetic transitions that involve them. Regarding the positive-parity states, they do not contain negative-parity bosons, except in the highest values of J, where the dimension of the subspace is strongly reduced. For instance, the 8^+ and 10^+ states in ^{214}Rn and ^{216}Rn, respectively, contain f_π bosons. This effect also appears in the other isotopes for higher values of J, although they are absent in Fig. 5. For this reason, calculations like the quadrupole moment that involve these states are not reliable. With respect to the relative neutron boson contents, the positive-parity bosons dominate the negative-parity bosons as A increases. The sum of the s_ν- and d_ν-boson contents is almost the same for the negative-parity states in each isotope, and the rest correspond to f_π-boson content, but as we move to heavier isotopes the ratio between the f_π-boson content and the s_ν- and d_ν-boson contents reduces. This effect is clear starting at ^{218}Rn and less pronounced in ^{214}Rn and ^{216}Rn, where again the states with the highest values of J depart from this systematic behavior. The p_ν-boson content is present only in the 1^- states, but in lower amounts than in the proton case. Only in ^{214}Rn is the p_ν-boson content comparable to the p_π-boson content.

In summary, we have used for the first time the $spdf$-IBM-2 model, which treats negative- and positive-parity configurations on equal footing. We applied this model to the chain of even-even isotopes from ^{214}Rn to ^{226}Rn, where octupole configurations are important. Also, this is the first time that a model has been applied to this chain, because previous studies have considered only the lightest members of this chain. The comparison of our calculations with the available experimental data is fair. More experimental data would be desirable to compare with the theoretical calculations and check the validity of this model. Only the lightest isotope, ^{214}Rn, shows some departures from the systematical behavior. Actually the chain of isotones that includes this isotope deserves a separate study, because the yrast 8^+ states show anomalous positions in the excitation spectra.

ACKNOWLEDGMENTS

This work was funded by the National Agency for Research and Development (ANID), FONDECYT Grant No. 1190489. We thank Stefan Heinze for supplying the ARBMODEL code [35] which was adapted to perform the calculations in this work.

APPENDIX

In this section we show how we obtained the parameters $\alpha_\rho^{(L)}$, $\beta_\rho^{(L)}$, and $\gamma_\rho^{(L)}$ in $Q_\rho^{(L)}$ for $L = 1$ and 3, corresponding to Eqs. (17) and (20). They are calculated when we map the shell model operators to the corresponding ones in the space of the IBM, specifically *spdf*-IBM-2:

$$Q_{\mathrm{SM},\rho}^{(L)} \mapsto Q_\rho^{(L)}.$$

The procedure is the same for protons ($\rho = \pi$) and neutrons ($\rho = \nu$). The only difference is the major shells where valence nucleons occupy the different single-particle levels. Hence we will omit the label ρ from now on. The shell model operator to map is explicitly

$$Q_{\mathrm{SM},M}^{(L)} = \sum_{p,q} \langle p \| r^L Y^{(L)} \| q \rangle (a_p^\dagger \tilde{a}_q)_M^{(L)},$$

where $Y_M^{(L)}$ is the spherical harmonic of degree L, and p and q refer to the quantum numbers that characterize the shell model single-particle states $|p, m_p\rangle = |n_p, l_p \frac{1}{2}, j_p, m_p\rangle$ and $|q, m_q\rangle = |n_q, l_q \frac{1}{2}, j_q, m_q\rangle$. $a_{p,m_p}^\dagger$ is the creation operator of a nucleon in the $|p, m_p\rangle$ state, and $\tilde{a}_{q,m_q} = (-1)^{j_q - m_q} a_{q,-m_q}$, where a_{q,m_q} is the annihilation operator of a nucleon in the $|q, m_q\rangle$ state. The IBM operators are

$$Q^{(L)} = \alpha^{(L)} [b_L^\dagger \tilde{s} + s^\dagger \tilde{b}_L]^{(L)} + \beta^{(L)} [p^\dagger \tilde{d} + d^\dagger \tilde{p}]^{(L)} + \gamma^{(L)} [f^\dagger \tilde{d} + d^\dagger \tilde{f}]^{(L)},$$

where b_L can be s, p, d, or f if $L = 0$, 1, 2, or 3, respectively. Following the OAI method [32], a mapping between shell model and IBM states is established:

$$|S^N; J = 0\rangle \mapsto |s^N; J = 0\rangle,$$
$$|S^{N-1} B_L; J = L\rangle \mapsto |s^{N-1} b_L; J = L\rangle,$$

where the shell model states are on the left-hand side and the IBM states are on the right-hand side, both of them normalized. N is half the number of valence nucleons. The shell model states are built from correlated pair operators $C_{LM}^\dagger$:

$$|S^N; J = 0\rangle = \frac{1}{\mathcal{N}_{N,0}} (C_0^\dagger)^N |0\rangle,$$
$$|S^{N-1} B_L; J = L\rangle = \frac{1}{\mathcal{N}_{N,L}} (C_0^\dagger)^{N-1} C_{LM}^\dagger |0\rangle,$$

where $\mathcal{N}_{N,L}$ is a normalization factor and

$$C_{LM}^\dagger = \sum_{p,q} c_{p,q}^{(L)} (a_p^\dagger \tilde{a}_q)_M^{(L)}.$$

The structure of the correlated pair operators is dictated by the coefficients $c_{p,q}^{(L)}$. They can be calculated using different means. We have obtained them from the components of the first state with the angular momentum L that arise when a surface delta interaction is diagonalized in the space of two particles, corresponding to a semimagic nucleus with two valence particles above (or two valence holes below) a closed shell. This calculation needs as input the energies of the single-particle levels used in the space of the two particles, which are taken from the excitation spectra of real semimagic nuclei with one nucleon above or below a closed shell. In our case, the use of bosons with negative parity implies the use of single-particle levels of both parities and hence one space that spans two major shells.

Once the shell model states are established firmly, the mapping to the IBM is performed by imposing the equality of matrix elements of the operators between the mapped states in each model. The matrix elements in the shell model were calculated using recurrence relations found in Ref. [36]. The matrix elements in the IBM are straightforward. Then, finally,

$$\alpha^{(L)} = \frac{\langle S^N; J = 0 \| Q_{\mathrm{SM}}^{(L)} \| S^{N-1} B_L; J = L\rangle}{\langle s^N; J = 0 \| Q^{(L)} \| s^{N-1} b_L; J = L\rangle},$$
$$\beta^{(L)} = \frac{\langle S^N D; J = 2 \| Q_{\mathrm{SM}}^{(L)} \| S^{N-1} P; J = 1\rangle}{\langle s^N d; J = 2 \| Q^{(L)} \| s^{N-1} p; J = 1\rangle},$$
$$\gamma^{(L)} = \frac{\langle S^N D; J = 2 \| Q_{\mathrm{SM}}^{(L)} \| S^{N-1} F; J = 3\rangle}{\langle s^N d; J = 2 \| Q^{(L)} \| s^{N-1} f; J = 3\rangle},$$

where we use S, P, D, and F for B_L with $L = 0$, 1, 2, and 3, respectively.

[1] J. Dobaczewski and J. Engel, Phys. Rev. Lett. **94**, 232502 (2005).
[2] J. Engel, M. J. Ramsey-Musolf, and U. van Kolck, Prog. Part. Nucl. Phys. **71**, 21 (2013).
[3] P. A. Butler, J. Phys. G: Nucl. Part. Phys. **43**, 073002 (2016).
[4] P. A. Butler and W. Nazarewicz, Rev. Mod. Phys. **68**, 349 (1996).
[5] S. G. Rohozinski, Rep. Prog. Phys. **51**, 541 (1988).
[6] N. Auerbach, V. Dmitriev, V. F. A. Lisetskiy, R. Sen' kov, and V. Zelevinsky, Phys. Rev. C **74**, 025502 (2006).
[7] V. V. Flambaum and V. G. Zelevinsky, Phys. Rev. C **68**, 035502 (2003).
[8] J. Engel, J. L. Friar, and A. C. Hayes, Phys. Rev. C **61**, 035502 (2000).
[9] K. Yanase, E. Teruya, K. Higashiyama, and N. Yoshinaga, Phys. Rev. C **98**, 014308 (2018).
[10] E. Teruya, K. Higashiyama, and N. Yoshinaga, Phys. Rev. C **93**, 064327 (2016); K. Higashiyama and N. Yoshinaga, EPJ Web Conf. **66**, 02050 (2014).

[11] Z. Y. Xu, Y. Lei, Y. M. Zhao, S. W. Xu, Y. X. Xie, and A. Arima, Phys. Rev. C **79**, 054315 (2009).
[12] N. V. Zamfir and D. Kusnezov, Phys. Rev. C **63**, 054306 (2001).
[13] N. V. Zamfir, Phys. At. Nucl. **64**, 1060 (2001).
[14] J. Engel and F. Iachello, Phys. Rev. Lett. **54**, 1126 (1985).
[15] J. Engel and F. Iachello, Nucl. Phys. A **472**, 61 (1987).
[16] T. Otsuka, Phys. Lett. B **182**, 256 (1986).
[17] T. Otsuka and M. Sugita, Phys. Lett. B **209**, 140 (1988).
[18] N. A. Smirnova, N. Pietralla, T. Mizusaki, and P. Van Isacker, Nucl. Phys. A **678**, 235 (2000).
[19] N. Pietralla, C. Fransen, A. Gade, N. A. Smirnova, P. von Brentano, V. Werner, and S. W. Yates, Phys. Rev. C **68**, 031305(R) (2003).
[20] N. Yoshinaga, T. Mizusaki, and T. Otsuka, Nucl. Phys. A **559**, 193 (1993).
[21] K. Nomura, D. Vretenar, and B.-N. Lu, Phys. Rev. C **88**, 021303(R) (2013); K. Nomura, D. Vretenar, T. Nikšić, and B.-N. Lu, *ibid.* **89**, 024312 (2014).
[22] M. Spieker *et al.*, Phys. Rev. C **97**, 064319 (2018).
[23] P. A. Butler, L. P. Gaffney, P. Spagnoletti *et al.*, Nat. Commun. **10**, 1 (2019); **11**, 3560 (2020).
[24] F. Iachello and A. Arima, *The Interacting Boson Model* (Cambridge University, Cambridge, England, 1987).
[25] R. J. Casperson, V. Werner, and S. Heinze, Phys. Lett. B **721**, 51 (2013).
[26] S.-C. Wu, Nucl. Data Sheets **110**, 681 (2009).
[27] S.-C. Wu, Nucl. Data Sheets **108**, 1057 (2007).
[28] A. K. Jain and B. Singh, Nucl. Data Sheets **107**, 1027 (2006).
[29] E. Browne and J. Tuli, Nucl. Data Sheets **112**, 1115 (2011).
[30] S. Singh, A. Jain, and J. K. Tuli, Nucl. Data Sheets **112**, 2851 (2011).
[31] L. Gaffney, P. A. Butler, M. Scheck *et al.*, Nature (London) **497**, 199 (2013).
[32] T. Otsuka, A. Arima, and F. Iachello, Nucl. Phys. A **309**, 1 (1978).
[33] J. Barea and F. Iachello, Phys. Rev. C **79**, 044301 (2009).
[34] C. Goodin *et al.*, Phys. Rev. C **79**, 034316 (2009).
[35] S. Heinze, Computer program ARBMODEL, 2008 (unpublished).
[36] F. Q. Luo and M. A. Caprio, Nucl. Phys. A **849**, 35 (2011).